International Journal of Microwave and Wireless Technologies

cambridge.org/mrf

Efficient modeling of a two-terminal polarization convertor–loaded dielectric-built filtenna using ML algorithms

Abhishek Kumar, Jitendra Ahir and Sanjeev Kumar Gupta

Department of Electronics and Communication Engineering, Ravindranath Tagore University, Bhopal, MP, India

Research Paper

Cite this article: Kumar A, Ahir J, Gupta SK (2025) Efficient modeling of a two-terminal polarization convertor–loaded dielectric-built filtenna using ML algorithms. *International Journal of Microwave and Wireless Technologies* **17**(10), 1875–1882. https://doi.org/10.1017/S1759078725102493

Received: 22 July 2025
Revised: 10 October 2025
Accepted: 17 October 2025

Keywords:
Alumina ceramic; filtering antenna; machine learning; multi-port radiator

Corresponding author: Abhishek Kumar; Email: abhishekphdrntu@gmail.com

Abstract

In this study, a metasurface (MS) polarization converter combined with a two-port dielectric antenna is constructed and studied. The feeding configuration, which consists of a printed line connected to an aperture, offers built-in filtering capabilities. In addition to converting linear to circular polarization between 2.49 and 3.25 GHz, the suspended MS layer enhances port isolation to less than −20 dB. In addition, the suggested radiator's |S11| is projected using the Random Forest and XGBoost machine learning (ML) models, which demonstrate satisfactory agreement with simulation data. The antenna effectively functions over 2.33–3.35 GHz, demonstrating that it is a leading contender for sub-6 GHz 5G communication systems. Fabricated measurements support both simulation and ML predictions.

Introduction

Modern wireless communication systems rely heavily on good antenna designs to function well. Well-optimized antennas enable increased data speeds, enhanced gain, and decreased alignment sensitivity. Circular polarization (CP) multi-port designs are especially beneficial since they increase data throughput using diversity methods without requiring more transmission power [1]. Additionally, CP reduces signal fading and guarantees orientation-independent communication [2]. Ceramic radiators are becoming more and more popular than traditional printed radiators because of their lower metallic losses, which allow for larger gain with fewer losses [3]. Simultaneously, the use of machine learning (ML) techniques is revolutionizing antenna creation by facilitating the quick and precise optimization of design parameters via the study of extensive performance data [4].

Multi-terminal ceramic radiators have been the subject of several investigations. By using polarization diversity in the 5.33–5.79 GHz range, Das et al. [5], for example, suggested a two-terminal ceramic radiator that is driven by a modified round slot and achieves isolation greater than −25 dB. Varshney et al. [6] developed a dual-terminal ceramic antenna that can generate rotational waves; it operates from 6.86 to 7.19 GHz and has a 3-dB ARBW across 6.98–7.11 GHz. Hu et al. [7] developed a 2-port ceramic antenna that operates from 2.38 to 2.57 GHz and accommodates cyclic radio waves between 2.41 and 2.53 GHz.A polarization converter allowed circular propagation between 5.53 and 5.99 GHz in a two-terminal ceramic antenna built by Abhay et al. [8] to be used in the 5.27–6.07 GHz region. Similarly, a metasurface (MS)-loaded two-terminal ceramic radiator spanning 5.17–5.45 GHz with a circular rotation inside 5.33–5.42 GHz was suggested by Gupta et al. [9]. A two-terminal slot-fed ceramic radiator that runs in the 4.13–4.59 GHz range and achieves circular rotation of the field from 4.17 to 4.45 GHz was suggested by Tripathi et al. [10]. To successfully lower the RCS within the operational range, an MS layer was included. Anitha et al. [11] planned a printed radiator in the mm-wave spectrum loaded with an MS (acts as a polarization convertor). It functions from 37.1 to 39.2 GHz with CP fields 38.2–38.6 GHz. Vankadhari et al. [12] suggested filtering radiator in the terahertz band, with the help of Silicon ceramic. It functions from 2.49 to 3.29 THz with circular fields within 2.59–2.89 THz.

The use of ML methods to radiator development and evaluation in the microwave spectrum has been the subject of various studies. These methods have shown promise in enhancing design as well as performance projection. For instance, Zheng et al. [13] used an AI model to precisely forecast the $|S_{11}|$ factor of a patch antenna so as to improve it. Sharma et al. [14] analyzed the efficacy of many ML techniques, such as Lasso regression, K-Nearest Neighbors (KNN), and Artificial Neural Network (ANN), to assess the performance of a T-formed printed radiator. Similarly, to improve the efficacy of a Ultra Wide Band (UWB) printed radiator, Ranjan et al. [15] used a variety of ML approaches. Srivastava et al. [16] used Knowledge-Based Neural Network (KBNNs) to overcome the drawbacks of traditional ANN models and precisely forecast the $|S_{11}|$. For an L-formed fed ring dielectric multi-port antenna intended to function with CP in the

© The Author(s), 2025. Published by Cambridge University Press in association with The European Microwave Association.

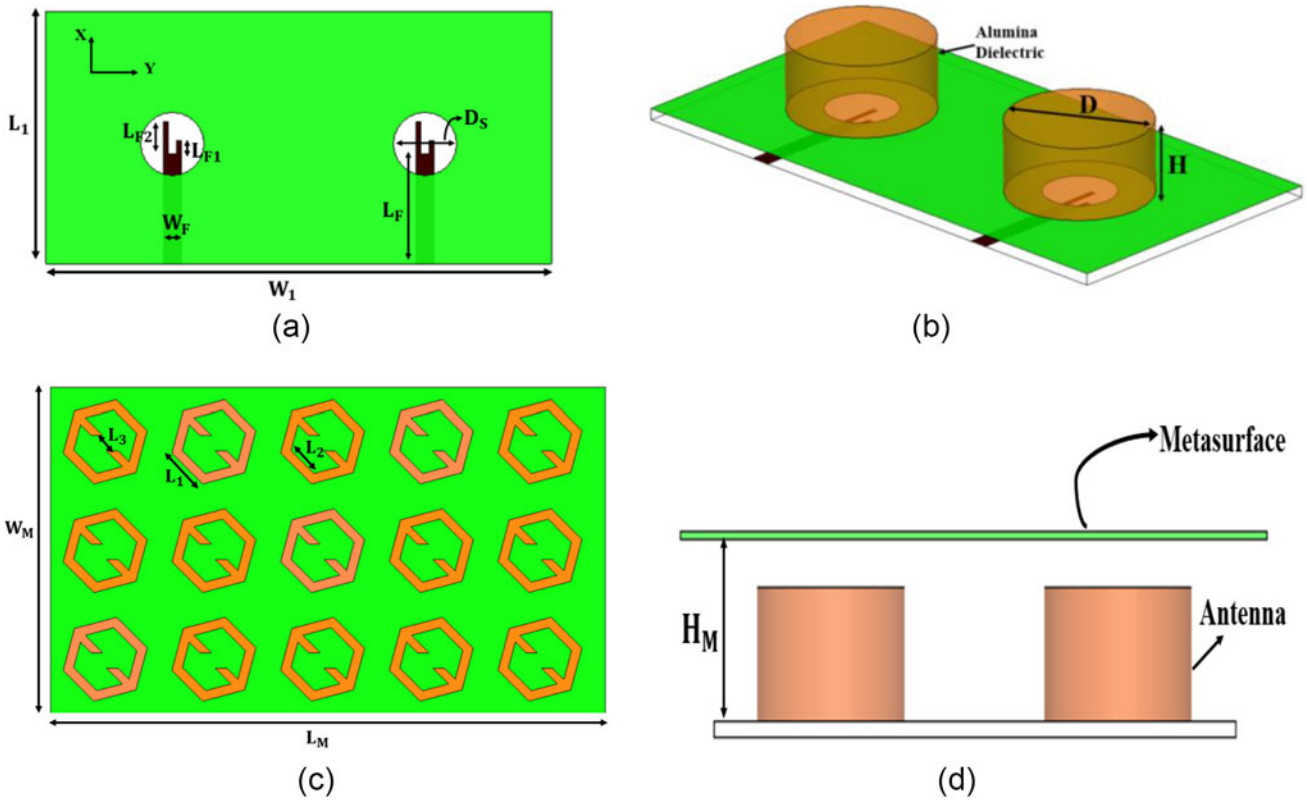


Figure 1. Design of the intended two-terminal antenna. (a) Feeding configuration. (b) Dielectric radiator. (c) MS layout. (d) Adjacent radiator sight.

Table 1. Optimum measurements of the planned two-terminal antenna's various components

Symbols	Size (mm)	Symbols	Size (mm)
W_1	78.0	D	18.0
L_1	48.0	H	8.5
L_F	10.5	H_M	15.5
W_F	2.5	L_{F1}	1.8
D_S	9.5	L_{F2}	4.8
L_1	11.5	L_2	10.75
L_M	84.0	W_M	88.0

2.8–3.05 GHz band, Pandey et al. [17] also used a variety of ML approaches. Dwivedi et al. [18] planned a two-terminal MS-loaded printed radiator in the mm-wave spectrum. ML approaches are used to predict the $|S_{11}|$ performance of the designed radiator.

The design and analysis of a two-port dielectric radiator with an MS incorporated is presented in this paper. The intended filtering response is achieved via a microstrip feed that has two unequal stubs. In addition to stimulating CP, the suspended MS enhances port isolation and lowers coupling to less than −25 dB. Additionally, XGBoost and Random Forest (RF) ML models are used to forecast the radiator's $|S_{11}|$. Novelty aspect of the planned radiator is as follows:

- Integration of suspended double-negative (DNG) MS with a ceramic antenna to achieve simultaneous circular waves, gain improvement, and filtering.

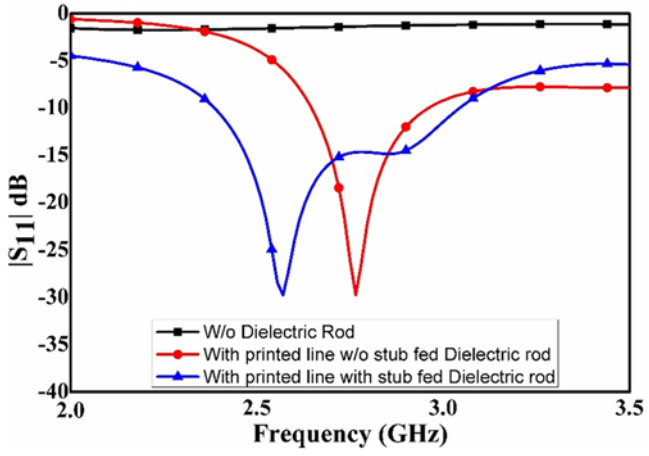


Figure 2. Curve of $|S_{11}|$ showing different changes to the solo terminal radiator's feed.

- Data-driven design validation using ML (RF, XGBoost) for predicting $|S_{11}|$, which is still rare in antenna design literature.

The article is organized into five parts for ease of reading: (a) antenna layout; (b) performance analysis; (c) prediction based on ML; (d) experiment confirmation; and (e) conclusion.

Antenna layout

The design of the suggested two-port dielectric radiator, shown in Fig. 1, is described in this section. The resonator of alumina

https://doi.org/10.1017/S1759078725102493 Published online by Cambridge University Press

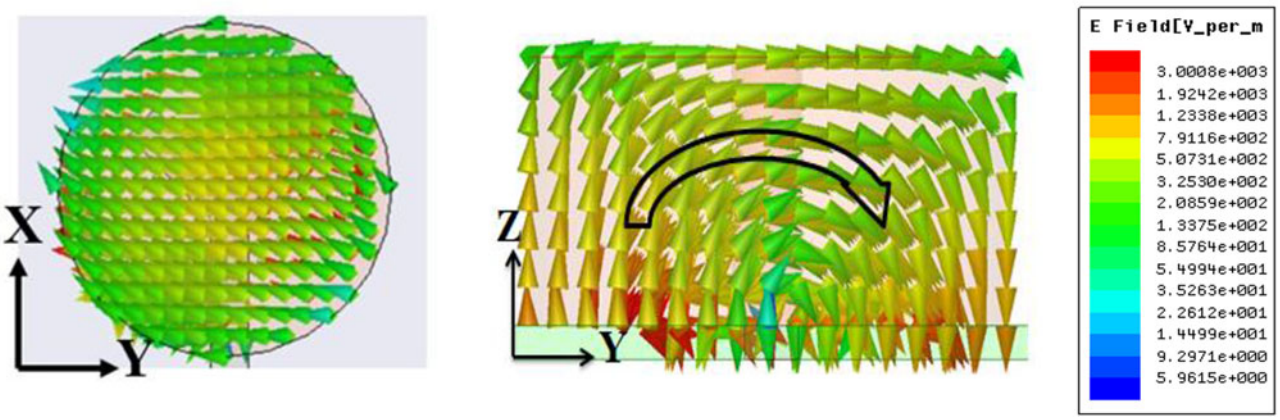


Figure 3. E-field patterns at 2.55 GHz on ceramic. (a) Upper sight. (b) Side sight.

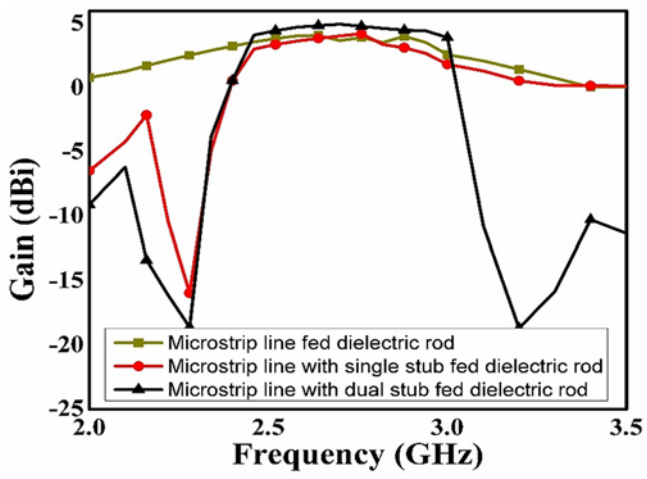


Figure 4. Curve of gain with several changes in the feed line.

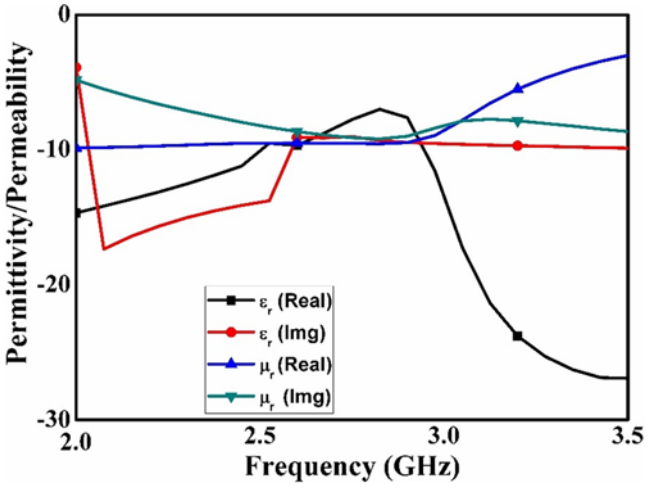


Figure 6. Curve of permittivity/permeability for the suggested unit cell.

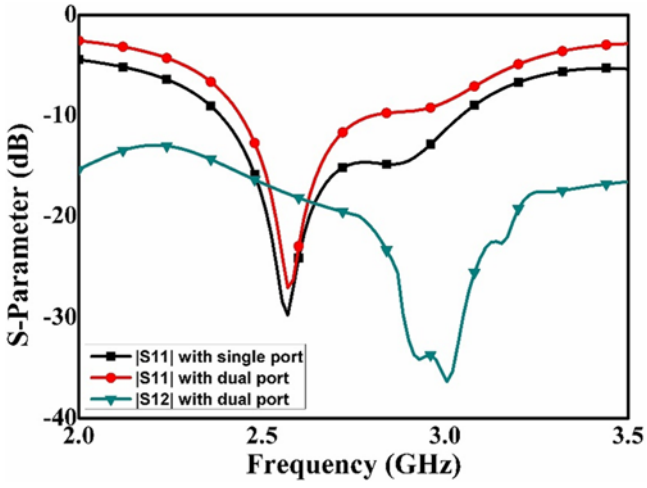


Figure 5. Curve of S-parameter with a solo/two-terminal antenna.

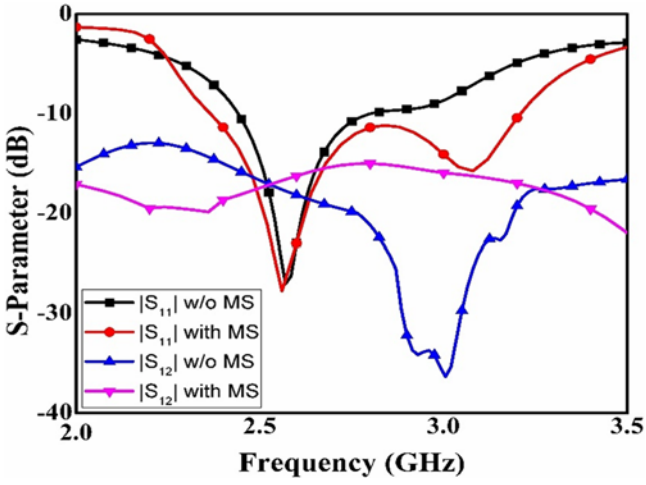


Figure 7. Curve of S-parameter presence and absence of MS.

($\mathcal{E}_r = 9.8$) is stimulated via a rounded slot that receives its input from a microstrip line that has two uneven stubs. The substrate of FR-4 ($\mathcal{E}_r = 4.4$, $H_S = 1.6$ mm) hosts the feed structure, with the ground plane on its top surface and the printed line on the bottom. To enhance performance, an MS, which is likewise made on FR-4, is hung above the radiator. Table 1 lists all of the important antenna parameters' optimal dimensions.

https://doi.org/10.1017/S1759078725102493 Published online by Cambridge University Press

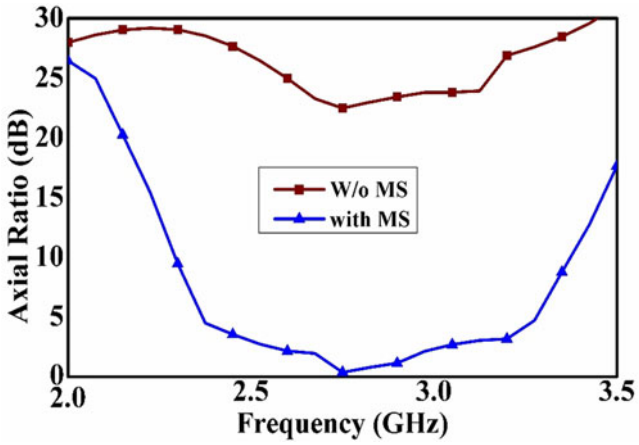


Figure 8. Curve of AR with and w/o MS.

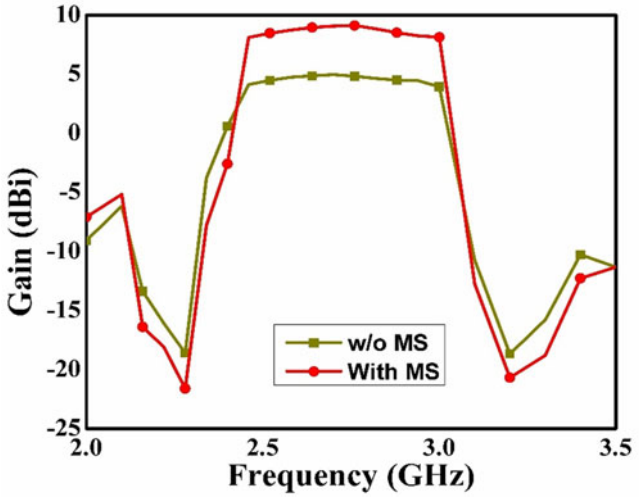


Figure 9. Curve of gain with and w/o MS.

Antenna investigation

This section provides a thorough HFSS analysis of the suggested antenna. First, a single-port radiator is used in the investigation. Figure 2 shows the $|S_{11}|$ response in the following three situations: (a) printed-line fed slot with no ceramic, (b) printed-line fed slot with a ceramic, and (c) printed line with dual-stub fed slot stimulating ceramic. Important findings from Fig. 2 include: (i) the ceramic is the primary source of the functional band, and (ii) the impedance BW is enhanced by the inclusion of stubs. Figure 3 presents the E-field distribution on the ceramic at resonance. The field pattern is similar to the basic $HEM_{11\delta}$ hybrid mode [19], which the slot excitation mechanism also supports. The following empirical equation may be used to estimate the mode [20]:

$$f_r = \frac{6.324c}{2\pi D\sqrt{\varepsilon+2}}\left\{0.27 + 0.36\left(\frac{D}{4H}\right) + 0.02\left(\frac{D}{4H}\right)^2\right\} \quad (1)$$

The dielectric rod's height and diameter are indicated by "D" and "H" in this equation, and its relative permittivity is shown by ε_r. In total, 2.43 GHz is the computed resonance derived from (1), and it closely resembles the resonance shown in the simulation findings.

Table 2. Evaluation of design in light of $|S_{11}|$ performance standards

Models	R^2 Score	MSE	MAE
RF	0.937	0.765	0.229
XGBoost	0.981	0.726	0.341

The gain fluctuation under three distinct situations is shown in Fig. 4. A dielectric rod is connected to a printed line-fed slot in (a), a single stub-fed slot-fed slot-coupled to the dielectric rod in (b), and two uneven stub-fed slots-coupled to the dielectric rod in (c). As can be seen from Fig. 4, the gain in instance (a) exhibits a smooth rise and fall across the band. The addition of a single elongated stub, however, drastically lowers the gain in example (b), bringing it below −15 dB at 2.25 GHz. When two unequal stubs are added in scenario (c), the gain is further suppressed to less than −20 dB at 3.25 GHz. The creation of radiation nulls at these frequencies is responsible for this decrease [18]. As a result, the suggested radiator has bandpass filtering properties.

By connecting the terminals in parallel, the single-terminal radiator may be expanded into a two-terminal setup. Figure 5 shows the relevant S-parameters. While the coupling in the two-terminal design is kept below −15 dB, it is evident that the $|S_{11}|$ response is almost the same in the solo and two-terminal situations. A unit cell is created and organized regularly to form an MS in order to further increase isolation. Figure 6 displays the unit cell's effective permittivity and permeability. Within the operational band, the permittivity is positive and the permeability is negative, indicating that the unit cell functions as a DNG MS. After that, this MS is hung above the radiator with two terminals. Figure 7, which displays the S-parameters with and without the MS, illustrates the effect of MS loading. Two important findings are noted: (a) the MS has little effect on the |S11| characteristics, and (b) the coupling between is also not much affected by the placement of MS.

The axial ratio (AR) properties with and without the MS are shown in Fig. 8. It is clear that adding the MS ensures CP by bringing the AR over the working range down to less than 3 dB. Because it divides the linear electric field into two perpendicular components of equal amplitude with a 90° phase difference, a necessary prerequisite for CP radiation, the proposed unit cell is fundamental to the generation of CP waves [21]. The broadside gain performance with and without the MS is shown in Fig. 9. The findings demonstrate that adding the MS raises the gain by around 3 dB, reaching an operating band maximum of 8.9 dBi. This improvement results from the DNG characteristic of the MS, which raises the directivity of the radiator [22].

$|S_{11}|$ prediction using ML methods

This section's goal is to demonstrate how ML methods may be used to estimate the $|S_{11}|$ properties of the suggested radiator. For this, two popular algorithms are used: XGBoost and RF. During training, RF, an ensemble-based ML technique, builds a lot of decision trees. Averaging (for regression tasks) or majority voting (for classification tasks) is used to combine the separate outputs from each tree to get the final prediction. A more sophisticated ensemble technique that makes use of the boosting idea

https://doi.org/10.1017/S1759078725102493 Published online by Cambridge University Press

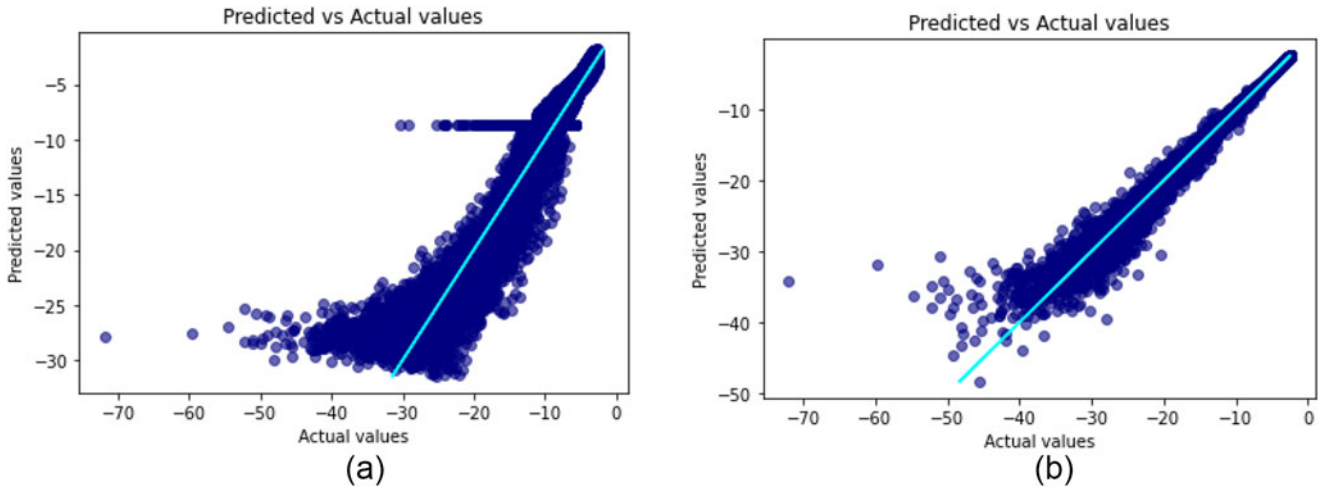


Figure 10. Comparison between expected and actual results $|_{11}|$. (a) XGBoost. (b) RF model.

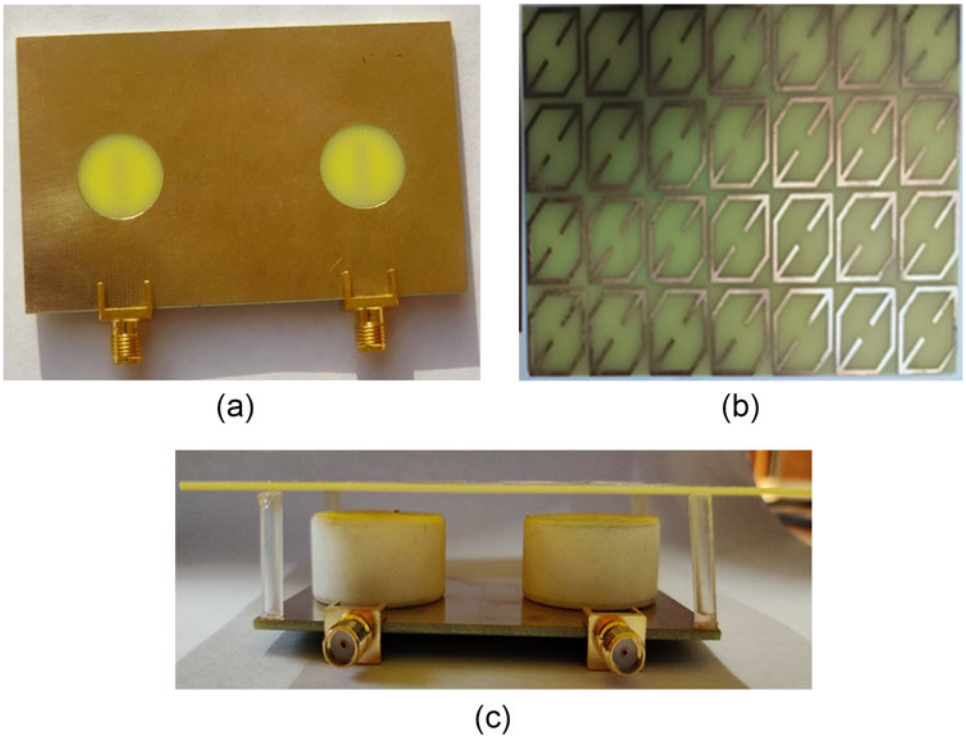


Figure 11. Images of the radiator archetype. (a) Feed assembly. (b) MS model. (c) Isometric sight.

is XGBoost. This method involves building many decision trees one after the other, with each new tree concentrating on fixing the mistakes (residuals) caused by the ones before it. When compared to many other ML algorithms, XGBoost is renowned for providing higher accuracy and quicker convergence because of its effective optimization method, regularization techniques, and scalability.

After the radiator was designed in HFSS, its geometric parameters were systematically changed to provide the necessary datasets. L_{F1} (0.3–4.25 mm), L_{F2} (1.5–8.5 mm), D_S (6.5–13.5 mm), D (15.0–25.0 mm), H (6.0–14.0 mm), H_M (12.0–19.0 mm), L_F (8.5–13.5 mm), and W_F (1.0–4.0 mm) were the arrays, in which parameters were changed using increments of 0.25 mm. In total, 101 evenly spaced sampling sites were used to conduct a frequency sweep throughout the 2.0–3.5 GHz range, yielding 124,667 data samples in total. Thirty percent of them were set aside for testing, and seventy percent were utilized to train the ML models.

The performance of the trained ML models is assessed using the test dataset. The findings are compiled in Table 2 for $|S_{11}|$ forecasts. With the greatest R^2 score and the lowest mean error in both scenarios, it is clear from these data that XGBoost performs better than RF.

Figure 10 shows the predicted vs real $|S_{11}|$ for the RF and XGBoost models. The ideal regression result, when predicted and actual values exactly correspond, is shown by the line Y = X. When

https://doi.org/10.1017/S1759078725102493 Published online by Cambridge University Press

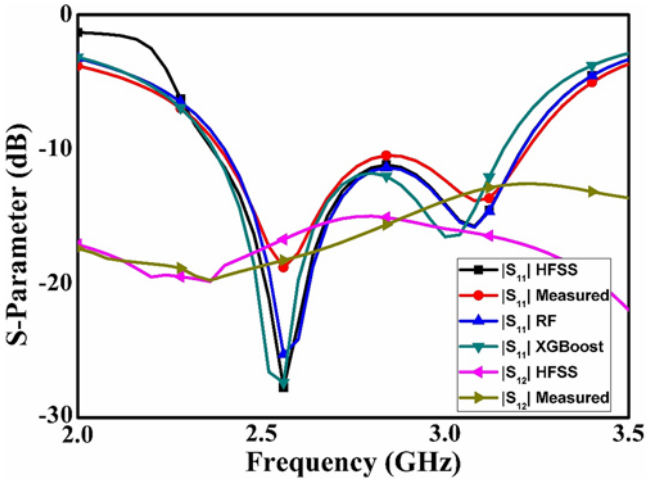


Figure 12. Tested/Simulated/Projected S-parameter curve.

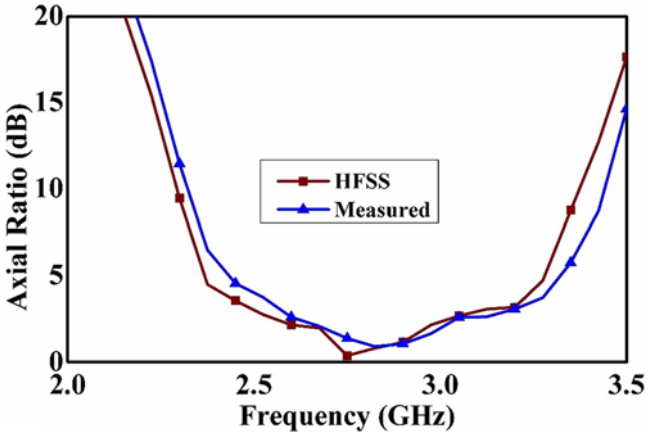


Figure 13. Tested/Simulated AR curve.

a greater density of data points closely matches this line, the model performs better. Out of the two models, XGBoost exhibits the best prediction accuracy with the closest alignment to the ideal line. The anticipated findings show growing discrepancies from the actual data as the values become increasingly negative.

Experimental verification

In this part, ML predictions and the improved simulation results are verified against real-world observations. The suggested radiator's manufactured prototype, created by a chemical etching method, is shown in Fig. 11. The ceramic rod is adhered to the substrate. The comparison of measured, simulated, and ML-predicted S-parameters is shown in Fig. 12. There is good agreement among the tested, simulated, and predicted outcomes. There is a slight shift seen between the tested and simulated ones, which is due to the use of glue to fix the ceramic, as well as due to the SMA connector. The antenna maintains a coupling level below −20 dB and functions well in a 2.33–3.35 GHz span.

The suggested radiator's tested and simulated AR is shown in Fig. 13. The dual-pattern measuring approach was used to assess the AR within an anechoic room [23]. The simulated and tested findings show a high degree of consistency. CP is maintained by the antenna across the 2.49–3.25 GHz span.

The LHCP/RHCP for terminals 1 and 2 in the XZ-plane at 2.7 GHz are shown in Fig. 14. There is a strong correlation between the simulated and measured polar plots. The graphs also support LHCP, and the broadside pattern confirms the excitation of the basic hybrid mode.

The suggested radiator's tested and simulated gain are shown in Fig. 15. The two-antenna method was used to measure the gain in an anechoic room [23]. Tested and simulated results show a significant connection. Within the functioning band, the radiator's gain is steady at about 8.9 dBi; however, outside of this range, it falls below −15 dB. The suggested design is contrasted with other documented two-terminal ceramic antennas in Table 3. The findings verify that the suggested radiator performs better overall in terms of gain, polarization, isolation, and bandwidth.

Figure 16 displays Diversity Gain (DG) and Envelop Corellation Coefficient (ECC) that were computed for the suggested radiator. ECC displays the correlation among the radiator's ports, whereas DG shows how well the antenna performs under fading channel circumstances. The DG should be nearly 10 dB and the ECC should be below 0.2 across the operational range for an efficient Multi

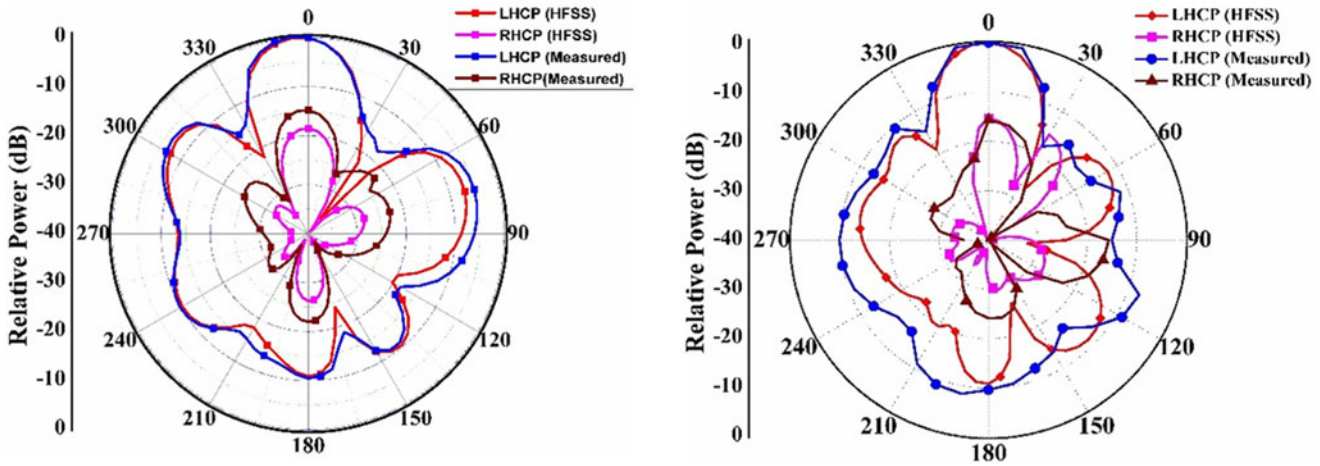


Figure 14. Polar graph of LHCP/RHCP at 2.7 GHz. (a) Port-1. (b) Port-2.

https://doi.org/10.1017/S1759078725102493 Published online by Cambridge University Press

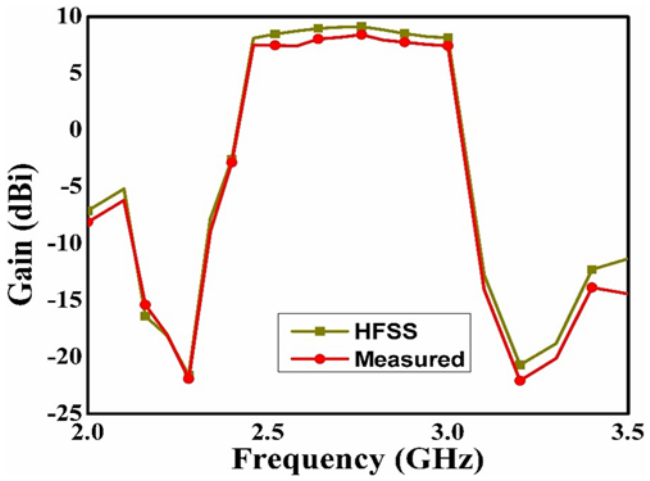


Figure 15. Tested/Simulated gain curve.

Table 3. Performance assessment of the proposed radiator against existing MIMO designs

Ref.	Working BW (GHz)	AR BW (GHz)	Gain (dBi)	ML technique	Isolation (dB)
[5]	0.56	0.19	5.8	–	20
[6]	0.39	0.29	2.9	–	15
[7]	0.19	0.14	6.2	–	20
[8]	0.59	0.19	5.9	–	20
[9]	0.29	0.08	3.3	–	20
[10]	0.51	0.31	4.1	–	20
[11]	0.33	0.19	3.9	–	20
[17]	0.25	0.12	4.4	Yes	25
[18]	0.48	0.18	5.1	Yes	20
Suggested radiator	1.02	0.78	8.9	Yes	20

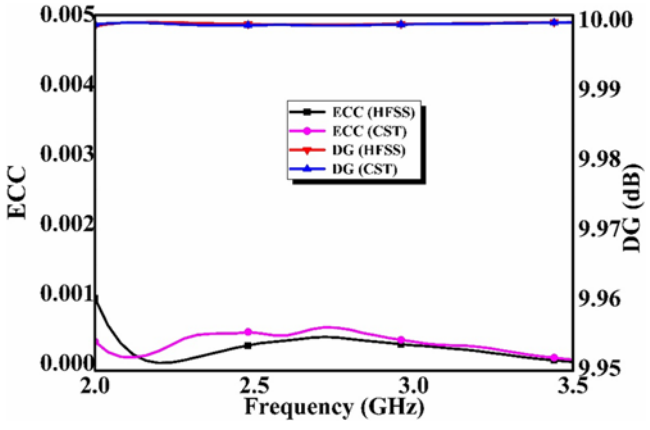


Figure 16. Measured/Simulated ECC/DG graph.

Input Multi Output (MIMO) antenna [24]. It is clear from Fig. 16 that the developed radiator meets these requirements, indicating that it is appropriate for MIMO applications.

Conclusion

The design and analysis of a two-port dielectric antenna with a suspended MS incorporated have been completed. By adding a filtering feature, the feed structure produces a gain of around 5.5 dBi within the operational range and suppresses it to approximately −15 dBi outside. The suspended MS improves the gain to above 8.5 dBi and permits CP in the 2.49–3.25 GHz span. The $|S_{11}|$ performance is also predicted using ML models. The fundamental hybrid mode is excited, which allows the antenna to function well in the 2.33–3.35 GHz range. Because of these features, the suggested architecture is ideal for 5G communication applications operating at frequencies lower than 6 GHz. Advantages of planned radiator are as follows:

- Feed design provides filtering characteristics
- Suspended MS improves the gain and creates CP waves within the operating regime
- Use of RF and XGBoost to predict $|S_{11}|$ is a novel contribution, reducing dependence on repetitive full-wave simulations

Limitations of the planned radiator are as follows:

- Precise alignment of the suspended MS and ceramic may introduce fabrication challenges.
- Use of glue for fixing the dielectric rod may affect repeatability and introduce minor uncertainties in measurements.

Funding statement. This research received no specific grant from any funding agency, commercial or not-for-profit sectors.

Competing interests. The authors report no conflict of interest.

References

1. **Sharawi MS** (2014) *Printed MIMO Antenna Engineering*. Boston, London: Artech House.
2. **Sharma A, Gupta S, Das G and Gangwar RK** (2020) Quad band quad sense circularly polarized dielectric resonator antenna for GPS/CNSS/WLAN/WiMAX applications. *IEEE Antennas and Wireless Propagation Letters* **19**, 403–408. https://doi.org/10.1109/LAWP.2020.2969743
3. **Petosa A** (2007) *Dielectric Resonator Antenna Handbook*. Norwood, MA, USA: Artech House.
4. **Misilmani HE, Naous T and Khatib SA** (2020) A review on the design and optimization of antennas using machine learning algorithms and techniques. *International Journal of RF and Microwave Computer-Aided Engineering* **30**, 1–7. https://doi.org/10.1002/mmce.22356
5. **Das G, Sharma A and Gangwar RK** (2018) Dielectric resonator based circularly polarized MIMO antenna with polarization diversity. *Microwave and Optical Technology Letters* **60**, 685–690.
6. **Varshney G, Singh R, Pandey VS and Yaduvanshi RS** (2020) Circularly polarized two-port MIMO dielectric resonator antenna. *Progress in Electromagnetics Research M* **91**, 19–28. https://doi.org/10.2528/PIERM20011003
7. **Hu Y, Pan YM and Yang MD** (2021) Circularly polarized MIMO dielectric resonator antenna with reduced mutual coupling. *IEEE Transactions on Antennas and Propagation* **69**, 3811–3819. https://doi.org/10.1109/TAP.2020.3048502
8. **Yadav AK, Verma S, Penmatsa KKV and Sharma A** (2023) Linear to circular polarized wave convertor loaded dual port Dielectric Resonator Antenna with enhanced gain for WLAN Applications. *Electromagnetics* **43**, 407–417. https://doi.org/10.1080/02726343.2023.2257525
9. **Gupta VK, Alam M, Yadav A and Sharma A** (2024) Two-port dielectric resonator antenna loaded with meta-surface for improving isolation and

circular polarization generator. *International Journal of Communication System* **37**, 1–10. https://doi.org/10.1002/dac.5676
10. **Tripathi M, Sharma A and Kumar V** (2024) Metasurface loaded dual port circularly polarized dielectric resonator antenna with reduced RADAR cross section and mutual coupling features. *Physica Scripta* **99**, 085501. https://doi.org/10.1088/1402-4896/ad5a54
11. **Anitha C, Singh V, Dwivedi AK and Narayanaswamy NK** (2024) Metasurface inspired printed dual-port MIMO antenna system with LP to CP conversion features for millimeter wave n260 band applications. *Scientific Report* **14**, 24437. https://doi.org/10.1038/s41598-024-75696-4
12. **Vankadhari H, Dwivedi AK, Singh V and Narayanaswamy NK** (2024) Design and investigation on circularly polarized tunable two port silicon ceramic-graphene based hybrid filtenna in THz frequency regime. *Optical and Quantum Electronics* **56**, 987–994. https://doi.org/10.1007/s11082-024-06443-2
13. **Zheng Z, Chen X and Huang K** (2010) Application of support vector machines to the antenna design. *International Journal of RF and Microwave Computer-Aided Engineering* **21**, 85–90. https://doi.org/10.1002/mmce.20491
14. **Sharma Y, Zhang HH and Xin H** (2020) Machine learning techniques for optimizing design of double t-shaped monopole Antenna. *IEEE Transactions on Antennas and Propagation* **68**, 5658–5663. https://doi.org/10.1109/TAP.2020.2966051
15. **Ranjan P, Maurya A, Gupta H, Yadav S and Sharma A** (2022) Ultra-Wideband CPW Fed Band-notched monopole antenna optimization using machine learning. *Progress in Electromagnetics Research M* **108**, 27–38. https://doi.org/10.2528/PIERM21122802
16. **Srivastava A, Gupta H, Dwivedi AK, Penmatsa KKV, Ranjan P and Sharma A** (2022) Aperture coupled dielectric resonator antenna optimization using machine learning techniques. *AEU- International Journal of Electronics and Communications* **154**, 1–9. https://doi.org/10.1016/j.aeue.2022.154302
17. **Pandey A, Singh AP and Kumar V** (2023) Design and optimization of circularly polarized dielectric resonator-based MIMO antenna using machine learning for 5G Sub-6 GHz. *AEU- International Journal of Electronics and Communications* **162**, 154558. https://doi.org/10.1016/j.aeue.2023.154558
18. **Dwivedi AK, Singh SK, Ranjan P, Sharma A and Singh V** (2024) Machine learning assisted dual port metasurface loaded MIMO antenna with linearly polarized to circularly polarized conversion features for n257 band of 5G mm-wave applications. *International Journal of Communication Systems* **37**, e5737. https://doi.org/10.1002/dac.5737
19. **Kajfez D, Glisson AW and James J** (1984) Computed modal field distributions for isolated dielectric resonators. *IEEE Transactions on Microwave Theory and Techniques* **32**, 1609–1616. https://doi.org/10.1109/TMTT.1984.1132900
20. **Sharma A, Das G and Gangwar RK** (2018) Composite antenna for ultra-wide bandwidth applications: exploring conceptual design strategies and analysis. *IEEE Antennas and Propagation Magazine* **60**, 57–65. https://doi.org/10.1109/MAP.2018.2818013
21. **Balanis CA** (2005) *Antenna Theory: Analysis and Design*. New York, USA: A John Wiley & Sons, INC., Publication.
22. **Samantaray D and Bhattacharyya S** (2020) A gain-enhanced slotted patch antenna using metasurface as superstrate configuration. *IEEE Transactions on Antennas and Propagation* **68**, 6548–6556. https://doi.org/10.1109/TAP.2020.2990280
23. **Stutzman GA and Thiele WL** (1998) *Antenna Theory and Design*, 2nd ed, Hoboken, NJ, USA: Wiley.
24. **Das G, Sharma A and Gangwar RK** (2018) Dielectric resonator based circularly polarized MIMO antenna with polarization diversity. *Microwave and Optical Technology Letters* **60**, 685–693. https://doi.org/10.1002/mop.31033



Abhishek Kumar received the B.E. and M.Tech. degrees in Electronics and Communication Engineering from Rajiv Gandhi Technical University (Govt.), India. He has more than five years of industry experience and is currently pursuing the Ph.D. degree in Electronics and Communication Engineering from Rabindranath Tagore University (RNTU), Bhopal, India. His research interests include electronic systems, communication technologies, embedded systems, VLSI design, and innovation in engineering design.



Jitendra Ahir received the B.Tech. degree in Electronics and Communication Engineering from Scope College of Engineering (RGPV University) Bhopal, the M.Tech. degree in Digital Communication from Scope College of Engineering (RGPV University) Bhopal, and the Ph.D. degree from Rabindranath Tagore University, Raisen, in the area of Microstrip Patch Antenna. He has more than 13 years of teaching and administrative experience.



Sanjeev Kumar Gupta received the B.E. degree in Electronics and Communication, the M.Tech. degree in Digital Communication, and the Ph.D. degree in Electronics and Communication Engineering from the University Institute of Technology (UIT), Barkatullah University Bhopal. In May 2000, he joined, AISECT group of Institutions. He has guided eight M.Tech. and thirteen Ph.D. research scholars. To his credit, four patents have been published. He has delivered a number of invited talks on many national platforms of repute. He has worked as an expert member in various committees of different institutions. He is also co-coordinating at Rabindranath Tagore University (formerly known as AISECT University) Bhopal. His current research interests include wireless communications, wireless sensor networks, control systems, microprocessors, and microcontrollers. He is a Fellow of the Institution of Electronics and Telecommunication Engineers (IETE). He organized various workshops, conferences, and faculty development programs. He has published 62 papers in National and International journals during his Ph.D. program at the university.

https://doi.org/10.1017/S1759078725102493 Published online by Cambridge University Press